ISSN 2070-2051, Protection of Metals and Physical Chemistry of Surfaces, 2021, Vol. 57, No. 3, pp. 525–534. © Pleiades Publishing, Ltd., 2021.

NANOSCALE AND NANOSTRUCTURED MATERIALS AND COATINGS

Evaluation of PEO Nanocomposite Coating on AZ31 Magnesium Alloy

M. Asgari[a], *, V. Torabinejad[a], M. R. Hoseini[b], Gh. Barati Darband[a], and A. Sabour Rouhaghdam[a]

[a] *Department of Materials Engineering, Tarbiat Modares University, Tehran, P.O. Box 14115-143 Iran*

[b] *Department of Chemistry, University of Isfahan, Isfahan, Isfahan, P.O. Box 81746-73441 Iran*

**e-mail: m_asgari23@yahoo.com*

Received May 4, 2020; revised August 24, 2020; accepted August 24, 2020

Abstract—The synthesis of ceramic coatings via conversion of metallic surface is the main route of corrosion resistance in the magnesium alloys. Using ceramic nano-particles as sealant in these coatings is very useful. In this study, the effect of applied current density and treatment duration on the alumina nanoparticle incorporation, corrosion resistance, and wear behavior of plasma electrolytic oxidation coating on AZ31 alloy was investigated. The results showed that the highest incorporation of nanoparticles occurs at a current density of 100 mA/cm^2 during 10 min while at higher current densities or treatment durations, the eruption of molten oxide prevents the embedding of nanoparticles inside the coating. The high incorporation of nanoparticles increased the homogeneity and compaction of the coating which caused the highest corrosion and wear resistance.

Keywords: plasma electrolytic oxidation, alumina nanoparticle, wear, corrosion

DOI: 10.1134/S2070205121030059

INTRODUCTION

Considering the low corrosion resistance of magnesium-based alloys, surface treatments are essential for industrial usage of these alloys. Plasma electrolytic oxidation (PEO) is the most effective technique used for the surface protection of magnesium and its alloys. Nanoparticle-embedded PEO coatings have attracted a lot of attention over the past few years [1, 2]. It is reported that nanoparticles filled the volcano-like valleys on the surface so that the difference between high and low areas was diminished. Also, some researches reported an improvement in corrosion and wear resistance by addition of alumina nanoparticles [3].

Almost all parameters that control the electrolysis process can affect the PEO process. Thus, current density is one of the most significant parameters that must be controlled during the PEO process [4]. Khan et al. [5], studied the effect of applied current density and electrolyte concentration on the surface morphology of PEO coating on Al and they reported that at low current densities (5 and 10 mA/cm^2), the coating showed porous coralline morphology and at higher current density (20 mA/cm^2) disrupted features were observed at the coating surface. Another important factor that influences PEO coating is duration. Duan et al. [6] studied the growth process of PEO coatings formed on AZ91D magnesium alloy. They showed that with increasing of treatment time, the thickness of PEO coatings and transfer resistance of ions and electrons were also increased.

Applied current density and coating duration time are two important factors that can affect the pores size and nanoparticle movement. To the best of our knowledge, the effect of applied current density and PEO duration time on nanoparticles incorporation have not been studied for PEO of AZ31 alloy. Thus, the aim of this study is to investigate the effect of applied current density and PEO duration on alumina nanoparticle incorporation, corrosion, and wear behavior of nanocomposite PEO coating.

EXPERIMENTAL

The AZ31 Mg alloy specimens were selected for PEO (Table 1). The PEO treatment was performed using the direct current and the cathode was made from stainless steel. The electrolyte composition used in the experiments includes 5 g/L $Na_3PO_4{\cdot}12H_2O$, 2 g/L KOH, and 30 g/L alumina nanoparticles (all of them were provided from MERCK). The TEM (Philips-CM120) image of alumina nanoparticles is shown in (a). The histogram of size distribution of alumina nanoparticles in the suspension with 30 g/L alumina, was determined by a dynamic light scattering spectroscopy (DLS; Malvern Instruments).

During the PEO process, a fixed rotation speed of 100 rpm was applied as the optimal electrolyte flow

Table 1. Chemical composition of used substrate

Element	Fe	Si	Ni	Mn	Cu	Zn	Al	Mg
wt %	0.001	0.01	0.002	0.64	0.01	0.9	3.5	Balance

rate [7]. In this study, the applied current density and test duration were adjusted in the range of 20–200 mA/cm^2 and 2.5–12.5 min, respectively. In order to study the effect of coating duration, the current density was optimized regarding the incorporation of nanoparticles. After that, PEO duration was evaluated at the fixed current density.

The samples were weighed before and after the PEO coating (micro-balance AND GR202, with the precision of ±50 μgr) and the weight change was calculated accordingly. The microstructure and morphology of PEO coatings were studied by scanning electron microscope (SEM, Philips XL30). The porosity of PEO surface and thickness of the coating were analyzed by JMicroVision 1.2.7 software. Corrosion behavior of the samples was evaluated against a 3.5 wt % NaCl solution by EG&G-273A potentiostat/galvanostat device. The potentiodynamic polarization test was carried out with a scan rate of 1 mV/s. Electrochemical impedance spectroscopy (EIS) was performed in the frequency range of 10^{-3}–65×10^3 kHz with the amplitude of ±10 mV around OCP. The pin-on-disk test was performed by a 45 N normal load with a total sliding distance of 200 m. The applied pin was made from an industrial polymer material called POLYGON which is a polymer-based composite material. The diameter of the spherical pin was 5 mm. The rotational speed and diameter were 100 rpm and 22 mm, respectively.

RESULTS AND DISCUSSION

Morphology and Microstructure

Applied current density is one of the important factors affecting microstructure, coating composition, and nanoparticle incorporation inside the coatings. After the entrance of the nanoparticles in the suspension and with the presence of hydroxide ions (OH^-), the negatively charged particles due to the electrical field, move toward the anode and are embedded inside the coating [8]. The change in weight percentage and thickness of the coatings are presented in 0, 3. As can be seen, by increasing applied current density, the coating thickness increases linearly probably due to the increase in the power of sparks and in turn driving force of coating [9]. Generally, by increasing the applied current density, the diameter of the micropores and eruption area of molten oxide increases and consequently the thickness of the coating will increase [5]. Moreover, by increasing the current density concentration of magnesium ions increases and causes the increase in interaction between magnesium and oxygen ions [10]. Increase in applied current density more than the critical value leads to the raising of coating porosity [9, 11]. It is also observed that the change in weight percentage of the coating increases up to the current density of 100 mA/cm^2 and reduced thereafter. Since other electrolyte variables are constant and the coating's thickness increases linearly, this observation can be due to the reduction of alumina nanoparticle incorporation at higher current densities as well as an increase in porosity. Therefore, it can be concluded that the highest incorporation occurs at current densities more than 100 mA/cm^2. Since the nanoparticles are neutral in the electrolyte, it can be expected that the decreased incorporation of nanoparticles cannot be justified by electrochemistry aspects. Due to the negative charge of nanoparticles, they move toward the anode as a result of electrophoretic force [12]. Furthermore, the high eruption of the molten oxide can be one of the main obstacles for incorporation of nanoparticles into the oxide layer [13]. By increasing either the applied voltage or current density [14], the spark power and volume of molten oxide increases which prevents the embedment of nanoparticles into the coating. It can be observed that by increasing the PEO duration, the coating weight increases up to 10 min and declines thereafter. It was also observed that the coating thickness increases until 10 min and then reaches a constant value. The increased weight percentage of the coating during the PEO process is caused by the incorporation of more nanoparticles and oxide layer growth. Since high energy is required to pass the current over the thick oxide layer [11], sparking on the surface becomes harder and the energy is concentrated on poor locations and sparks occur in these locations. Thus, the number of micro-pores is reduced and their size becomes larger, probably leading to the reduced incorporation of the nanoparticles in these pores. Hence, it can be concluded that the highest incorporation of the nanoparticles occurs for PEO duration of 10 min.

The SEM images at different current densities are shown in Fig. 4. As is shown, the applied current density is effective on the morphology and microstructure. The micro pores and cracks in these coatings originated from the eruption of molten oxide and thermal stresses during the solidification [15, 16]. It can be seen from Fig. 4 and the cross-section images that the cracks and imperfections are fewer in the case of the PEO coating fabricated at a current density of 100 mA/cm^2. The reason for which seems to be due to the highest incorporation of nanoparticles [7].

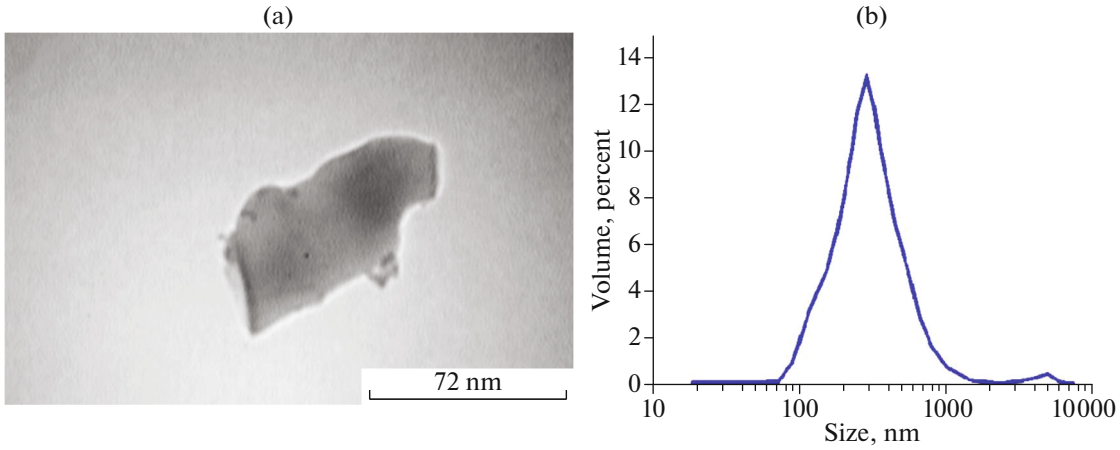

Fig. 1. (a) TEM image of used alumina nanoparticles, (b) the histogram of size distribution in suspension of alumina nanoparticles.

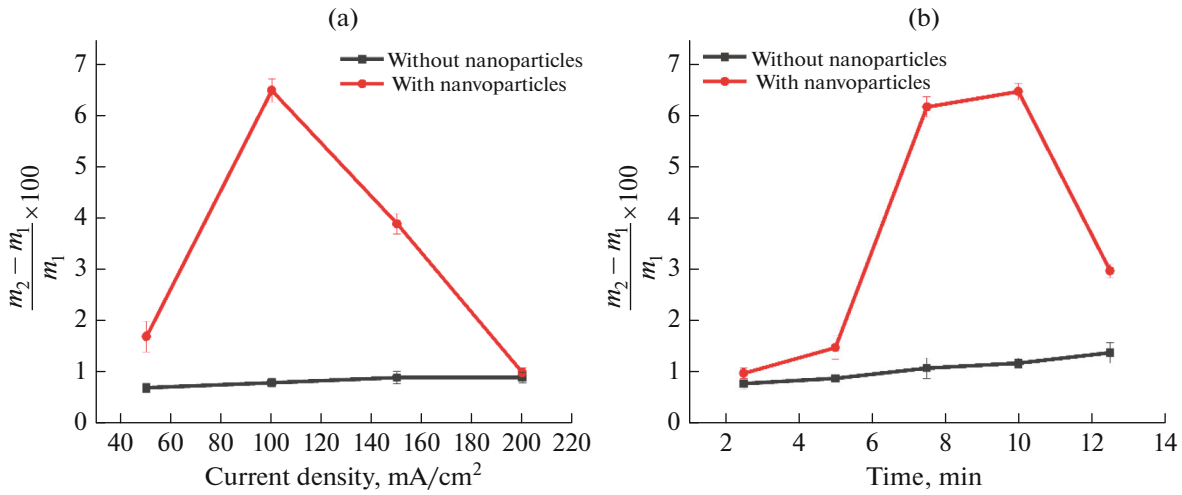

Fig. 2. Variation of coating weight percentage (a) versus applied current density (PEO coating duration was maintained fixed at 10 min) and (b) versus PEO duration (current density was maintained fixed at 10 mA/cm^2).

The SEM images of the coated specimens for different treatment times are shown in Fig. 5, where some microspores and surface cracks are observed. As mentioned above, by being adsorbed at high energy sites such as microcracks and micro-pores, nanoparticles reduced the coating's porosity. Furthermore, the cross-sectional images indicate that the coating and substrate adhesion is properly high and content of discontinuities and defects is very low in the interface.

In order to study the chemical composition of coatings, the EDS analysis from a cross-section of coatings with and without nanoparticles is shown in Fig. 6. In the coating without nanoparticles, the main elements in the coatings are Mg, O, and P. These elements originate from compounds which are formed during PEO treatment. Homogenous distribution of all elements across the coating can be seen. Elemental mapping of coating with nanoparticles showed the presence of Al that originates from alumina nanoparticles and indicating the incorporation of alumina nanoparticles inside the coating from the electrolyte.

Corrosion Resistance of the Coating

Potentiodynamic Polarization

The polarization curves of coatings are shown in Fig. 7 (a). The results of corrosion resistance, corrosion current density (i_{corr}), and corrosion potential (E_{corr}) were extracted from the polarization curves (through drawing Tafel slopes) [17]. As shown in Table 2 the optimum corrosion resistance occurs at the applied current density of 100 mA/cm^2. In PEO coatings, the oxide layer acts as a barrier and prevents the contact between the corrosive ions in the solution and

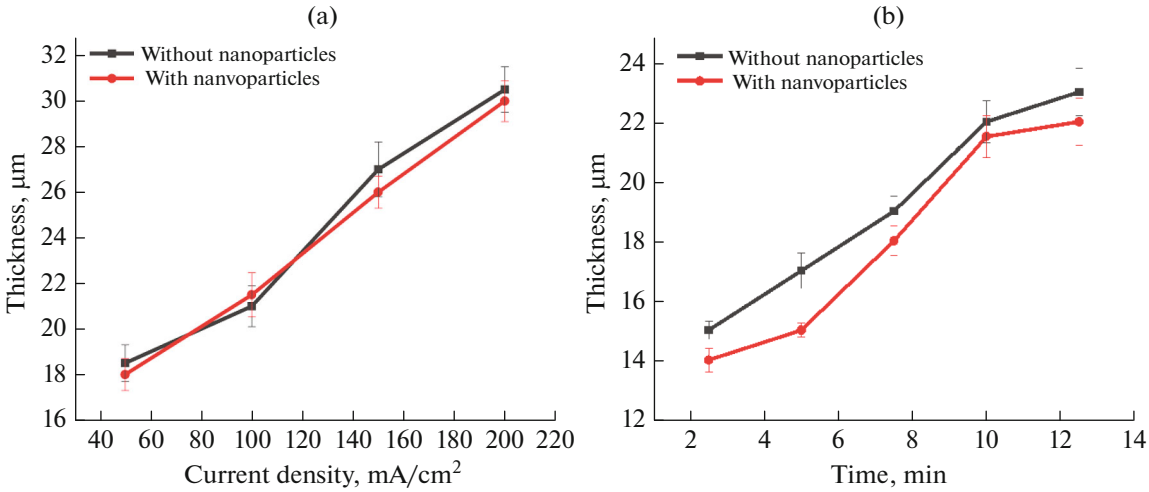

Fig. 3. Variation of coating's thickness (a) versus applied current density (PEO coating duration was maintained fixed at 10 min) and (b) versus PEO duration (current density was maintained fixed at 10 mA/cm^2).

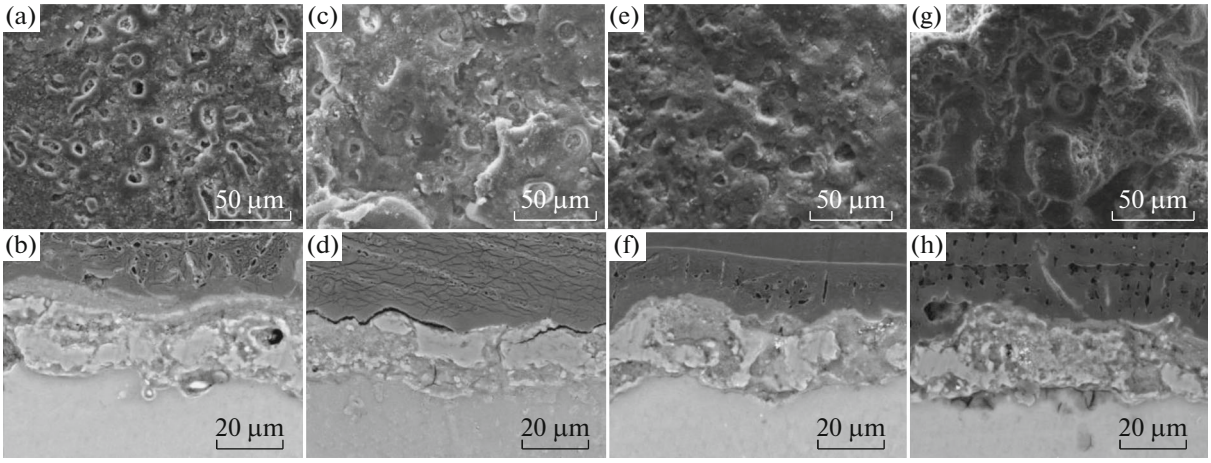

Fig. 4. The SEM micrographs from top and cross section of PEO coatings fabricated by applying current densities of (a, b) 50, (c, d) 100, (e, f) 150, and (g, h) 200 mA/cm^2 at constant duration of 10 min.

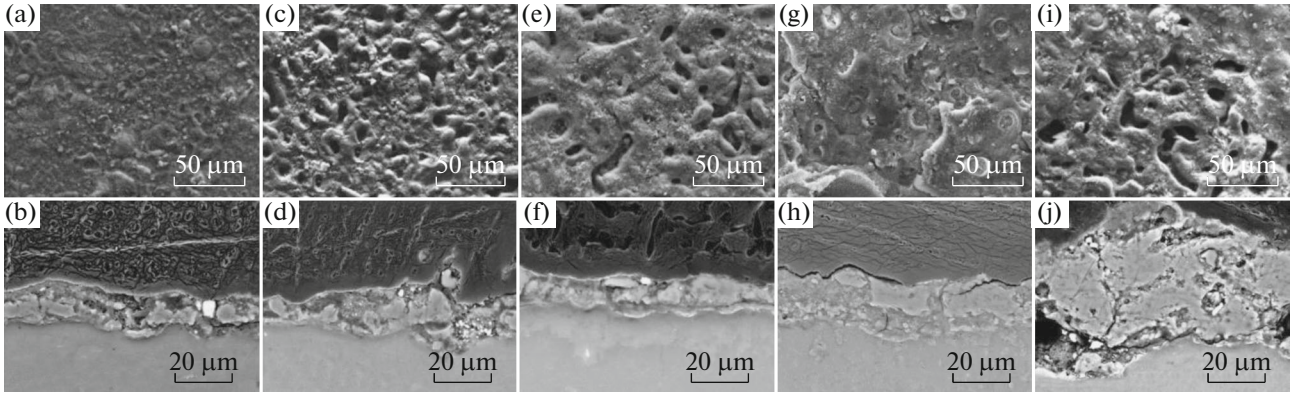

Fig. 5. The SEM micrographs of top and cross section of different PEO coatings fabricated at (a, b) 2.5, (c, d) 5, (e, f) 7.5, (g, h) 10, (i, j) 12.5 min at current density of 100 mA/cm^2.

Table 2. Parameters extracted from polarization curves in various applied current densities

Current density, mA/cm^2	β_a, mV/decade	β_c, mV/decade	i_{corr}, μA/cm^2	R_p, kΩ cm^2	Corrosion rate, mpy	E_{corr}, mV vs. SCE
Bare Mg	65.727	113.473	31.02	0.583366	28.17	−1583
50	209.414	231.2	19.93	1.881784	23.07	−1540
100	63.64	35.849	0.5119	15.28934	0.5924	−1509
150	180.108	57.966	2.63	5.690893	3.044	−1494
200	146.179	190.296	20.26	1.392721	23.44	−1549

Table 3. Parameters extracted from polarization curves in various operation times

Time, min	β_a, mV/decade	β_c, mV/decade	i_{corr}, μA/cm^2	R_p, kΩ cm^2	Corrosion rate, mpy	E_{corr}, mV vs. SCE
12.5	190.337	28.804	1.489	5.73	1.724	−1430
10	63.64	35.849	0.5119	15.28	0.5924	−1509
7.5	136.693	49.346	1.4	8.839	1.62	−1485
5	127	55	1.7	7.705	2.07	−1524
2.5	207	27	1.2	6.793	0.777	−1495
Bare Mg	65.727	113.473	31.02	0.583	28.17	−1583

Table 4. Parameters extracted from EIS curves in various applied current densities

Current density, mA/cm^2	R_s, Ω cm^2	n_2	CPE_2, Ω^{-1} cm^{-2}	R_2, (Ω cm^2)	n_1	CPE_1, Ω^{-1} cm^{-2} ($\times 10^{-6}$)	R_1, Ω cm^2	L
50	32	0.28	0.00109	319	0.68	1.34	1234	28
100	30	0.31	0.00014	5500	0.72	3.03	35000	36330
150	32	0.01	0.0005	100	0.65	9.2	7500	2000
200	34	0.135	0.0036	9900	0.55	7.00	899	63.4

the substrate and reduces the corrosion rate of the substrate [18]. Therefore, by decreasing the porosity of the oxide layer and increasing of its density, diffusion of corrosive ions into the surface will be lowered [19]. Moreover, the higher incorporation of the nanoparticles in the coating improved corrosion resistance. Nanoparticles were adsorbed on the coating defects such as micropores and cracks and by filling these defects prevented the entrance of aggressive ions toward the substrate [7, 20, 21]. The polarization curves of the coatings at different PEO durations are shown in Fig. 7 (b), while the extracted variables from the polarization tests are exhibited in Table 3 (all tests repeated three times and their averages were reported). It is observed that the lowest corrosion current density which is equivalent to the highest corrosion resistance is achieved after 10 min. Layer properties such as density are among the most important factors affecting the corrosion resistance of an oxide layer. It is observed in the SEM images that the highest nanoparticle's incorporation occurs at this time, at which the penetration of corrosive ions into the substrate is prevented. As is expected the highest corrosion resistance belongs to this coating.

Electrochemical Impedance Spectroscopy

Nyquist curves related to the coated specimens at various current densities are presented in Fig. 8. The semicircle diameter and total impedance indicate the corrosion resistance. It is observed that the largest semicircle diameter and the maximum total impedance at low frequencies are in the current density of 100 mA/cm^2 which correspond to the highest corrosion resistance. There is a good agreement between the PDP and EIS with the maximum corrosion resistance of coated specimen at 10 min PEO duration.

To interpret EIS results, an equivalent electrical circuit was fitted for the EIS curves. The parameters extracted from these curves are shown in Table 4. As it can be observed, the equivalent electrical circuit has two constant phase elements. The first constant phase

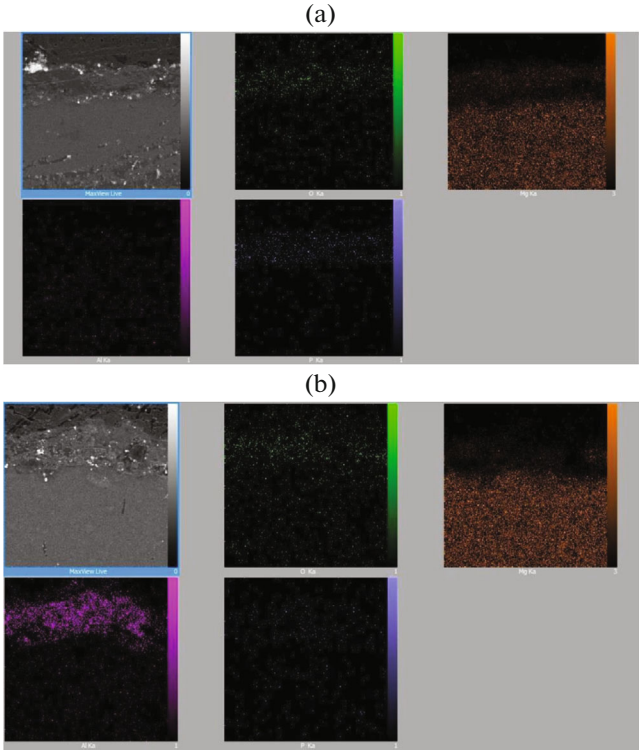

Fig. 6. The EDS elemental mapping of PEO coated samples by current density of 100 mA/cm^2 and duration of 10 min (a) in electrolyte free of nanoparticles and (b) in suspension of 30 g/L alumina nanoparticles.

element in the range of low frequency is related to the dense layer in the PEO process while the second constant phase element at high-frequency range is associated with the outer layer (porous layer). In the equivalent fitted circuit, R_s represents the solution resistance, R_1 indicates outer layer (porous layer) resistance, CPE_1 is the constant phase element in the outer layer (porous layer), R_2 is the inner layer (dense layer) resistance, and CPE_2 is the constant phase element in the outer layer (porous layer). The presence of the induction loop in these curves may indicate pitting due to the outer layer (porous layer). The heterogeneity of surface and surface roughness can also affect the corrosion behavior. In this regard, the rough surface showed low corrosion resistance. In general, in the EIS parameters, n represents the roughness and it is close to 1 when the surface roughness becomes lower. Table 5 shows that the highest value of n in the specimens is obtained at 10 min of PEO duration and the current density of 100 mA/cm^2. The incorporation of nanoparticles in the coatings led to the surface homogeneity and inhibited the penetration of corrosive ions and thus raised the corrosion resistance [22].

Wear Resistance

Various parameters such as porosity, cracks in the coating, roughness and coating thickness affect the wear properties of the coating [23]. The wear rate of specimens coated at different PEO condition is shown

Table 5. Parameters extracted from EIS curves for the samples coated at various operation times

Time, min	R_s, Ω cm^2	n_2	CPE_2, Ω^{-1} cm^{-2}	R_2, Ω cm^2	n_1	CPE_1, (Ω^{-1} cm^{-2}) ($\times 10^{-6}$)	R_1, Ω cm^2	L
12.5	32	0.33	0.00078	190	0.57	11	16800	4526
10	30	0.31	0.00014	5500	0.72	3.03	35000	36330
7.5	32	0.05	0.00054	100	0.58	1.09	14483	5700
5	34	0.44	3.55E–05	2500	0.585	2.7	9500	250
2.5	32	0.64	0.00088	1000	0.62	2.4	9500	1000

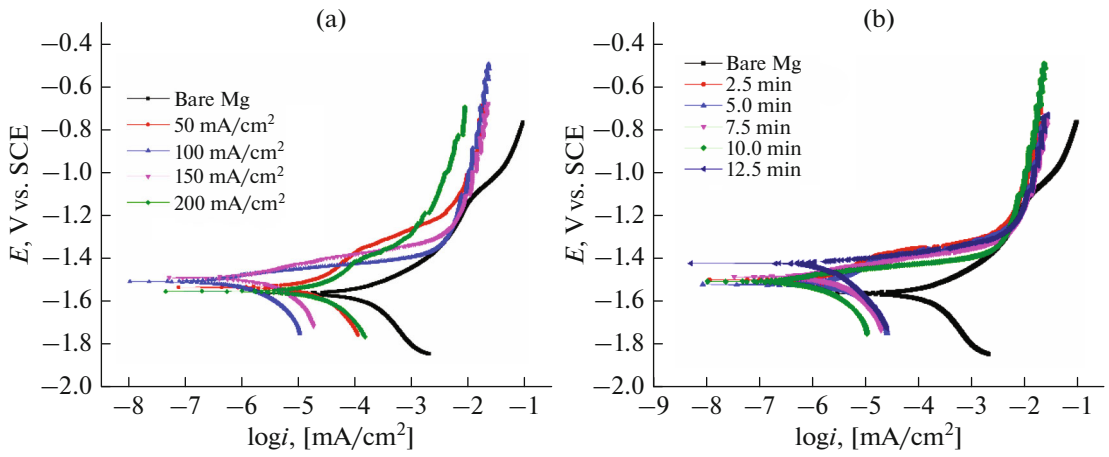

Fig. 7. The polarization curves of PEO coatings fabricated at (a) different applied current densities with constant duration of 10 min and (b) different PEO durations at fixed 100 mA/cm^2 current density.

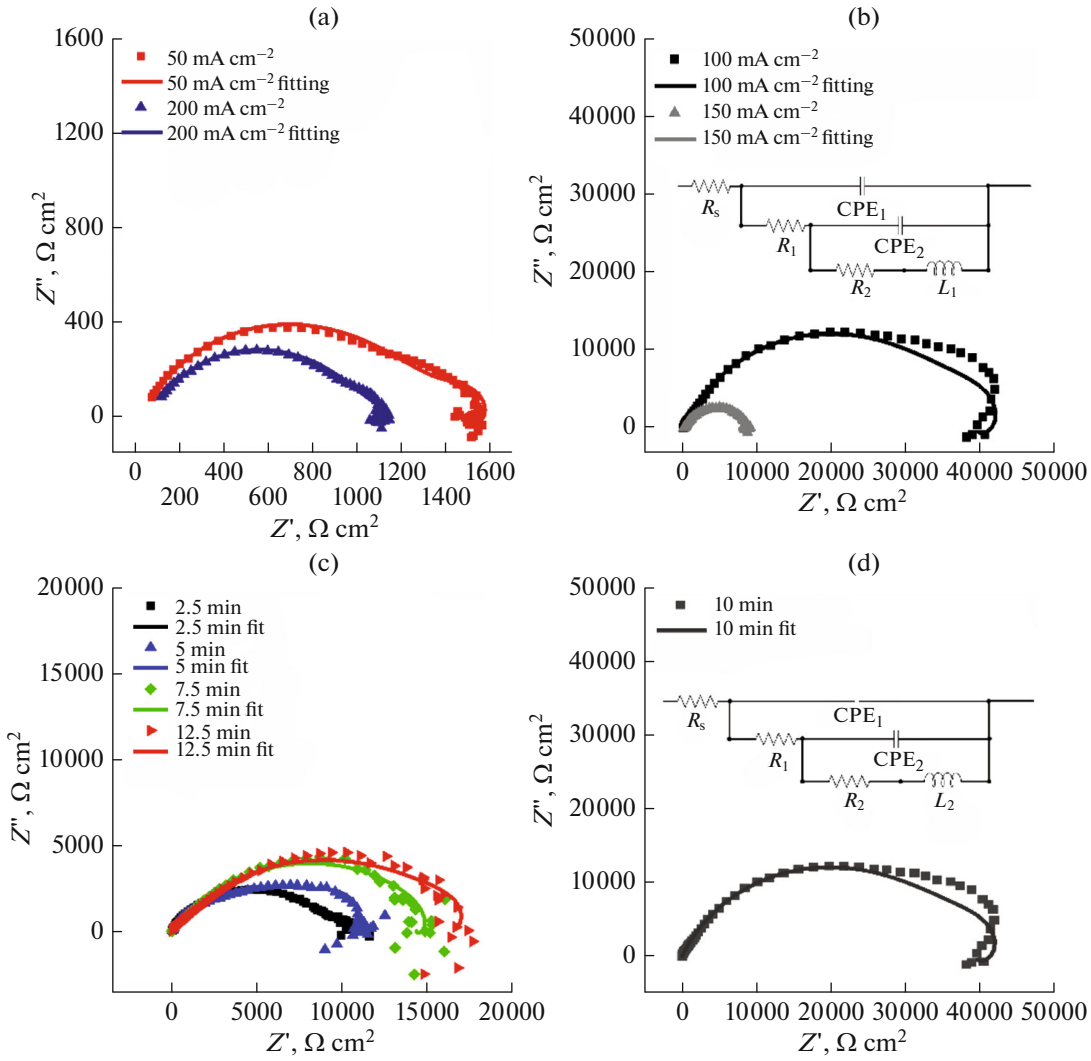

Fig. 8. Nyquist curves of coatings fabricated at (a) different applied current densities at fixed coating duration of 10 min, (b) different PEO coating durations at fixed 100 mA/cm^2 of current density.

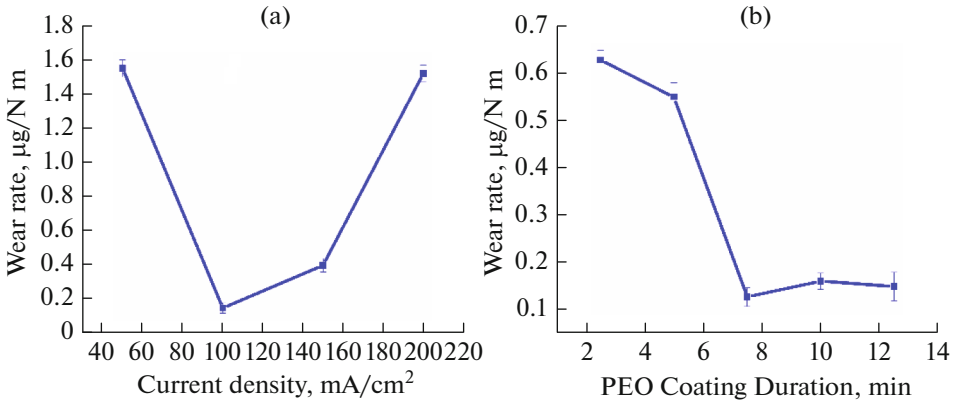

Fig. 9. The variation of wear rate (a) versus applied current density at fixed PEO coating duration of 10 min, (b) versus PEO coating duration at fixed 100 mA/cm^2 of current density.

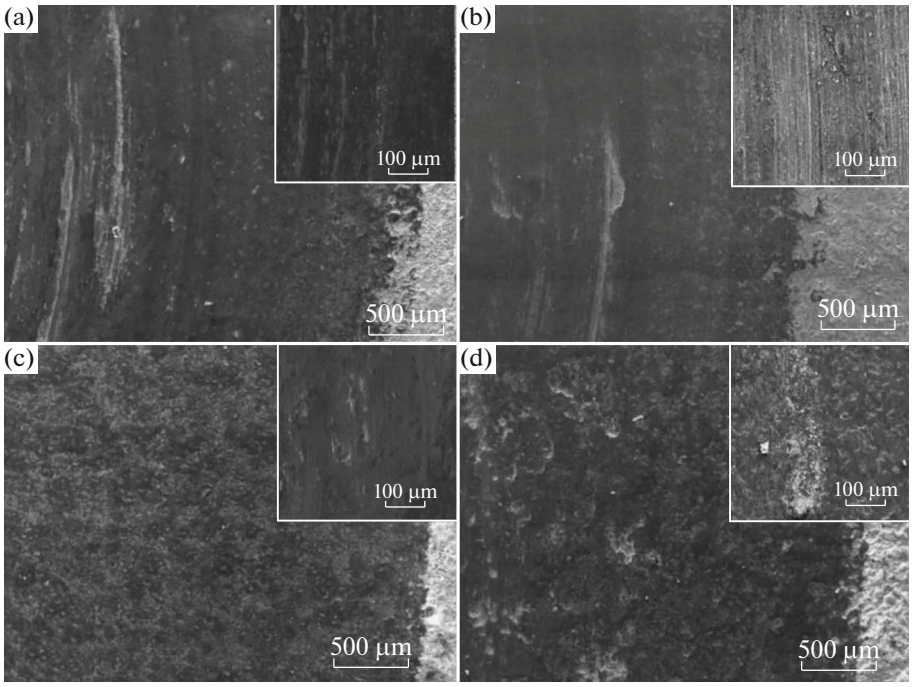

Fig. 10. SEM images of worn surfaces of PEO coatings fabricated by applying (a) 50, (b) 100, (c) 150, (d) 200 mA/cm^2 of current density at fixed coating duration of 10 min.

in Fig. 9. As it is clear from Fig. 9 (a), the lowest wear rate is for the specimens coated at a current density of 100 mA/cm^2. The trend of wear rate from low to high wear rate is 100, 150, 200, and 50 mA/cm^2. This pattern corresponds to the nanoparticle incorporation at different applied current densities presented in Fig. 6 and indicates that as nanoparticle incorporation in the coating is reduced, the wear rate is increased [24].

Figure 9 (b) shows the trend of wear rate at different PEO times shown and suggests that as the nanoparticle incorporation in the coating is decreased, the wear rate is increased because the concentration of hard alumina nanoparticles increased hardness and strength of coatings and reduced the porosity of coating [25]. The SEM images of the specimens after the wear test are shown in Figs. 10 and 11. It can be seen that the coating with low incorporation of alumina nanoparticles is fully worn after the wear test and even reaches the magnesium alloy substrate. Samples with high incorporation of alumina nanoparticles have abrasive wear mechanism (samples coated at 100 mA/cm^2 and 10 min). In the case of samples with low incorporation of alumina nanoparticles, the dominant wear mechanism is adhesive (samples coated at current densities of 50 and 200 mA/cm^2 and time process-

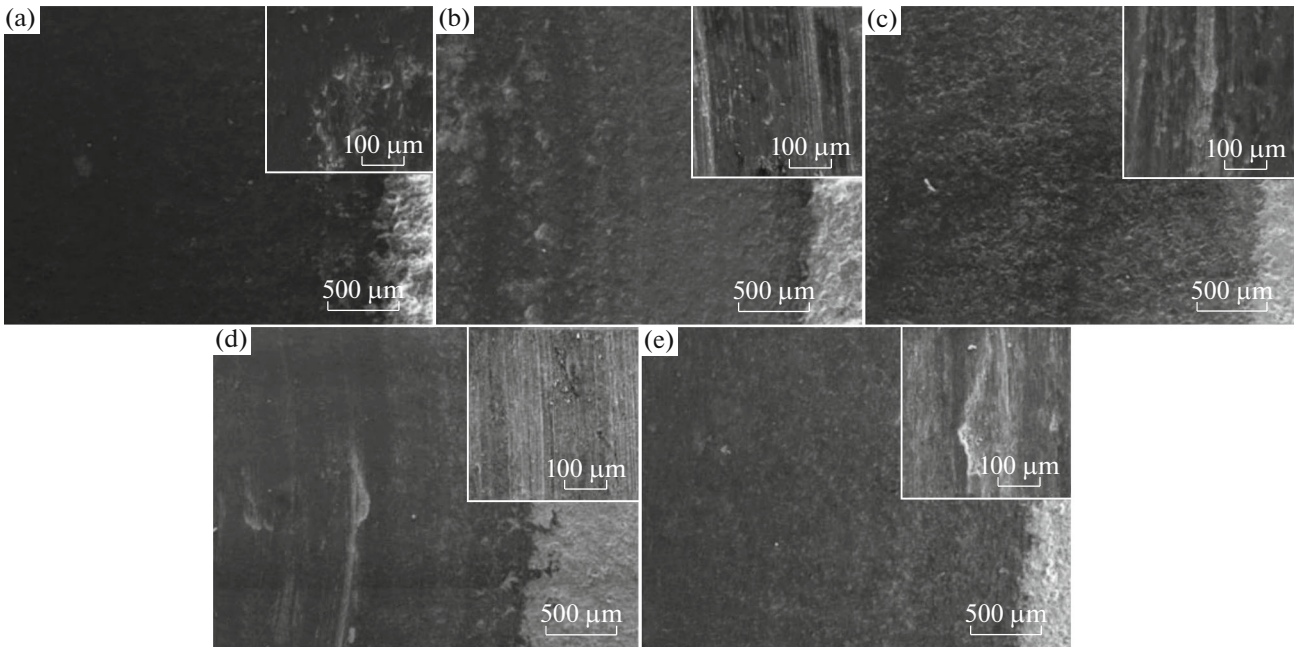

Fig. 11. SEM images of worn surfaces of PEO coatings fabricated at (a) 2.5, (b) 5, (c) 7.5, (d) 10 min of coating duration at fixed 100 mA/cm^2 of current density.

ing of 2.5 and 12.5 min). The dominant wear mechanism for other samples is a mixture of abrasive and adhesive. As the SEM images suggest, by adding the nanoparticles to the coating the porosities in the coating are reduced, leading to the improved wear rate of coatings [26]. Yu et al. [27] reported the porosities in their studies and stated that these areas lead to the cracking, crushing, and delamination of the coating over the wear process. Generally, it is believed that the wear in PEO coating is adhesive wear and by incorporation of hard nanoparticles, the type of wear is changed to abrasive wear.

CONCLUSIONS

In this study, the effects of applied current density and PEO duration time are studied. The results of this study showed that the highest incorporation of nanoparticles occurs at the current density of 100 mA/cm^2 and 10 min of PEO duration. In comparison, at higher current densities, the eruption of molten oxide prevents the penetration of nanoparticles into the coating and at the PEO duration of 10 min, the increase in the thickness of the coating causes spark concentration on weak spots and reduces the number of sparks, preventing the proper incorporation of the nanoparticles. High incorporation of nanoparticles under such conditions increases the density and uniformity of the coatings and in turn improvement of the corrosion and wear resistance. The high content of nanoparticles and its effect on the properties of the coating has an optimum condition that was achieved at the current density of 100 mA/cm^2 and PEO duration of 10 min.

REFERENCES

1. Aliofkhazraei, M., Rouhaghdam, A.S., and Gupta, P., *Crit. Rev. Solid State Mater. Sci.,* 2011, vol. 36, no. 3, pp. 174–190. https://doi.org/10.1080/10408436.2011.593269
2. Soliman, H. and Hamdy, A., *Surf. Eng.,* 2017, vol. 33, no. 10, pp. 767–772.
3. Zhuang, J.J., Song, R.G., Xiang, N., et al., *Surf. Eng.,* 2017, vol. 33, no. 10, pp. 744–752. https://doi.org/10.1080/02670844.2016.1190123
4. Li, Q., Liu, C., Yang, W., et al., *Surf. Eng.,* 2017, vol. 33, no. 10, pp. 760–766.
5. Khan, R.H.U., Yerokhin, A., Li, X., et al., *Surf. Coat. Technol.,* 2010, vol. 205, no. 6, pp. 1679–1688. https://doi.org/10.1016/j.surfcoat.2010.04.052
6. Duan, H., Yan, C., and Wang, F., *Electrochim. Acta,* 2007, vol. 52, no. 15, pp. 5002–5009.
7. Asgari, M., Aliofkhazraei, M., Darband, G.B., et al., *Surf. Coat. Technol.,* 2017, vol. 309, pp. 124–135. https://doi.org/10.1016/j.surfcoat.201611.050
8. Lu, X., Blawert, C., Zheludkevich, M.L., et al., *Corros. Sci.,* 2015, vol. 101, pp. 201–207. https://doi.org/10.1016/j.corsci.2015.09.016
9. Hussein, R.O., Northwood, D.O., and Nie, X., *J. Vac. Sci. Technol., A,* 2010, vol. 28, no. 4, pp. 766–773. https://doi.org/10.1116/1.3429583
10. Bala Srinivasan, P., Liang, J., Blawert, C., et al., *Appl. Surf. Sci.,* 2009, vol. 255, no. 7, pp. 4212–4218. https://doi.org/10.1016/j.apsusc.2008.11.008

11. Durdu, S. and Usta, M., *Appl. Surf. Sci.,* 2012, vol. 261, pp. 774–782. https://doi.org/10.1016/j.apsusc.2012.08.099
12. Song, Y.L., Sun, X.Y., and Liu, Y.H., *Mater. Corros.,* 2012, vol. 63, no. 9, pp. 813–818. https://doi.org/10.1002/maco.201106251
13. Aliofkhazraei, M., Sabour Rouhaghdam, A., and Shahrabi, T., *Surf. Coat. Technol.,* 2010, vol. 205, pp. S41–S46. https://doi.org/10.1016/j.surfcoat.2010.03.052
14. Qiu, Z., Wang, R., Zhang, Y., et al., *J. Mater. Eng. Perform.,* 2015, vol. 24, no. 4, pp. 1483–1491.
15. Guo, H.F. and An, M.Z., *Appl. Surf. Sci.,* 2005, vol. 246, nos. 1–3, pp. 229–238. https://doi.org/10.1016/j.apsusc.2004.11.031
16. Gu, C., Wang, L., Hu, X., et al., *Surf. Eng.,* 2017, vol. 33, no. 10, pp. 773–778. https://doi.org/10.1080/02670844.2017.1287622
17. Gheytani, M., Aliofkhazraei, M., Bagheri, H.R., et al., *J. Alloys Compd.,* 2015, vol. 649, pp. 666–673. https://doi.org/10.1016/j.jallcom.2015.07.139
18. Cao, F.H., Cao, J.L., Zhang, Z., et al., *Mater. Corros.,* 2007, vol. 58, no. 9, pp. 696–703. https://doi.org/10.1002/maco.200704050
19. Darband, G.B., Afshar, A., and Rabani, M., *J. Alloys Compd.,* 2016, vol. 688, pp. 596–604.
20. Torabinejad, V., Aliofkhazraei, M., Rouhaghdam, A.S., et al., *Surf. Eng.,* 2016, vol. 33, no. 2, pp. 122–130. https://doi.org/10.1080/02670844.2016.1151577
21. Wang, P., Gong, Z.Y., Hu, J., et al., *Surf. Eng.,* 2018, vol. 35, no. 117, pp. 1–8. https://doi.org/10.1080/02670844.2018.1557996
22. Ji, R., Ma, M., He, Y., et al., *Ceram. Int.,* 2018, vol. 44, no. 13, pp. 15192–15199. https://doi.org/10.1016/j.ceramint.2018.05.159
23. Wu, X., Su, P., Jiang, Z., et al., *ACS Appl. Mater. Interfaces,* 2010, vol. 2, no. 3, pp. 808–812. https://doi.org/10.1021/am900802x
24. Yu, L., Cao, J., and Cheng, Y., *Surf. Coat. Technol.,* 2015, vol. 276, pp. 266–278. https://doi.org/10.1016/j.surfcoat.2015.07.014
25. Aliofkhazraei, M. and Rouhaghdam, A.S., *Surf. Coat. Technol.,* 2011, vol. 205, pp. S57–S62.
26. Wang, Y., Jiang, B., Guo, L., et al., *Appl. Surf. Sci.,* 2006, vol. 252, no. 8, pp. 2989–2998.
27. Yu, L., Cao, J., and Cheng, Y., *Surf. Coat. Technol.,* 2015, vol. 276, pp. 266–278.